

Delayed entanglement echo for individual control of a large number of nuclear spins

Zhen-Yu Wang, Jorge Casanova, and Martin B. Plenio

Institut für Theoretische Physik and IQST, Albert-Einstein-Allee 11, Universität Ulm, D-89069 Ulm, Germany

Methods for achieving quantum control and detection of individual nuclear spins by single electrons of solid-state defects play a central role for quantum information processing and nano-scale nuclear magnetic resonance (NMR)^{1–8}. However, with standard techniques, no more than 8 nuclear spins have been resolved^{2–4,9,10}. Here we develop a new method that improves significantly the ability to spectrally resolve nuclear spins and demonstrate its capabilities with detailed numerical simulations by using a nitrogen-vacancy (NV) centre¹¹ as model system. Based on delayed entanglement control, a technique combining microwave and radio-frequency (rf) fields, nuclei with resonances in a broad frequency band can be unambiguously¹² and individually addressed by the sensor electron. Additionally the spectral resolution can extend beyond the electron spin relaxation time by using a long-lived qubit memory. Our method greatly increases the number of useful register qubits accessible to a defect centre and improves the signals of nano-scale NMR.

Nuclear spins are natural quantum bits with long coherence times for quantum information tasks¹³ and they encode information about the structure of molecules and materials in a form that is accessible to NMR techniques¹⁴. The NV centre in diamond represents a promising nano-scale platform for detection and coherent control of such nuclear spins^{9,11}. In type IIa diamonds, the decoherence of the NV electron spin is dominated by the presence of ¹³C nuclei. However, when properly controlled, the ¹³C nuclear spins in the vicinity of an NV centre become useful resources^{5–7}. Furthermore, NV centres can be implanted close to the diamond surface to detect the signal of nuclear spins above the surface^{15,16}, which opens opportunities for both quantum information processing^{6,7,17} and single molecule NMR¹⁶ when environmental noise can be controlled.

Originally developed in NMR, dynamical decoupling (DD) techniques^{14,18} can extend significantly qubit coherence times and they can also be applied to address single nuclear spins by an NV centre^{2–4,8,19–21}. Nevertheless standard DD techniques can only be used to address a few nuclear spins because of a number of drawbacks such as low spectral resolution¹⁰, resonance ambiguities¹², and perturbations from the electron-nuclear coupling²⁰. In this respect correlation spectroscopy could improve the resolution by measuring the NV signal over long evolution times¹⁰, however this technique does not provide advantages on individual spin addressing and control.

Our method overcomes these difficulties by selectively addressing target nuclear spins by radio-frequency (rf) fields in a delay window while the entanglement with the electron spin sensor is preserved by a subsequent Hahn echo¹⁴ operation. In this manner highly selective entangling gates between the electron spin and different target nuclear spins can be achieved.

Now we describe the details of our method. A magnetic field B_z parallel to the NV symmetry axis splits the spin triplet of the orbital ground electronic state of the NV centre. We use two of the three levels $m_s = 0, \pm 1$ to define an NV electron spin qubit¹¹. Under strong magnetic fields such that the nuclear Zeeman energies exceed the perpendicular components, A_j^\perp , of the hyperfine field \mathbf{A}_j at the locations of nuclear spins, see Fig. 1a, the interaction between the NV electron spin and its surrounding nuclear spins is described by

$$H_{\text{int}} = \sigma_z \otimes \eta \sum_j A_j^\parallel I_j^z.$$

with $\sigma_z = |\uparrow_e\rangle\langle\uparrow_e| - |\downarrow_e\rangle\langle\downarrow_e|$. Here we use $|\uparrow_e\rangle = |m_s = +1\rangle$ as one of the qubit states while the second qubit state may be $|\downarrow_e\rangle = |m_s = 0\rangle$, when $\eta = 1/2$, or $|\downarrow_e\rangle = |-1\rangle$ with $\eta = 1$ (see Supplementary Information). For each nuclear spin, A_j^\parallel denotes the component of \mathbf{A}_j parallel to the nuclear spin quantisation axes (see Fig. 1a,b). The nuclear precession frequencies are shifted by A_j^\parallel , which can be used to address individually nuclear spins of the same species (homonuclear spins).

An initial superposition state of the electron spin $|\psi_e\rangle = c_\uparrow|\uparrow_e\rangle + c_\downarrow|\downarrow_e\rangle$ loses its coherence because of the electron-nuclear coupling H_{int} . This effect can be removed by the Hahn echo. In our case, a microwave π pulse exchanges the states $|\uparrow_e\rangle \leftrightarrow |\downarrow_e\rangle$ and effectively reverses $H_{\text{int}} \rightarrow -H_{\text{int}}$. When the evolutions before and after the π pulse have the same duration τ , entanglement from all the nuclear spins is erased, preserving the electron spin coherence.

In order to preserve the coupling with a target spin, we apply rf-driving at the precession frequency of the target spin during a delay window. By flipping the target spin j by an angle $\theta_{\text{rf}} = \pi$, we selectively rephase its interaction with the electron spin and realize a quantum gate

$$|\uparrow_e\rangle\langle\uparrow_e| \otimes U_+ + |\downarrow_e\rangle\langle\downarrow_e| \otimes U_-$$

with $U_\pm = \exp(\mp 2i\eta\tau A_j^\parallel I_j^z)$, up to single spin rotations. This leads to the possibility of creating entanglement between the electron spin and selected nuclear spins which forms a key ingredient of our method. Note that it is not essential that $\theta_{\text{rf}} = \pi$ as almost any choice of

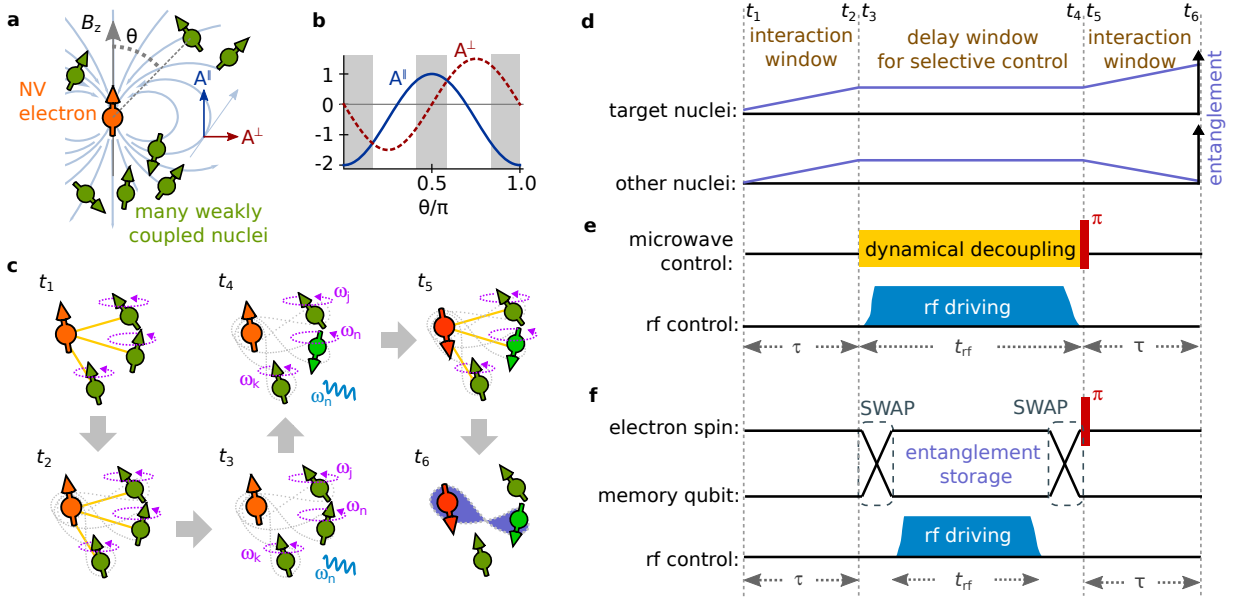


Figure 1: **Delayed entanglement control between the NV electron and its surrounding nuclear spins.** **a**, A large number of nuclear spins weakly coupled to the electron spin of NV centre by the hyperfine field. **b**, Relative amplitudes of the components of the hyperfine field. The perpendicular component A^\perp is weaker than the parallel component A^\parallel at the shaded regions of the plot. **c**, Illustration of the spin states in the process of delayed entanglement echo, with the entanglement changes sketched in **d**. Implementation of the delay window by DD (**e**) or by storing the entanglement to a long-lived memory qubit (**f**).

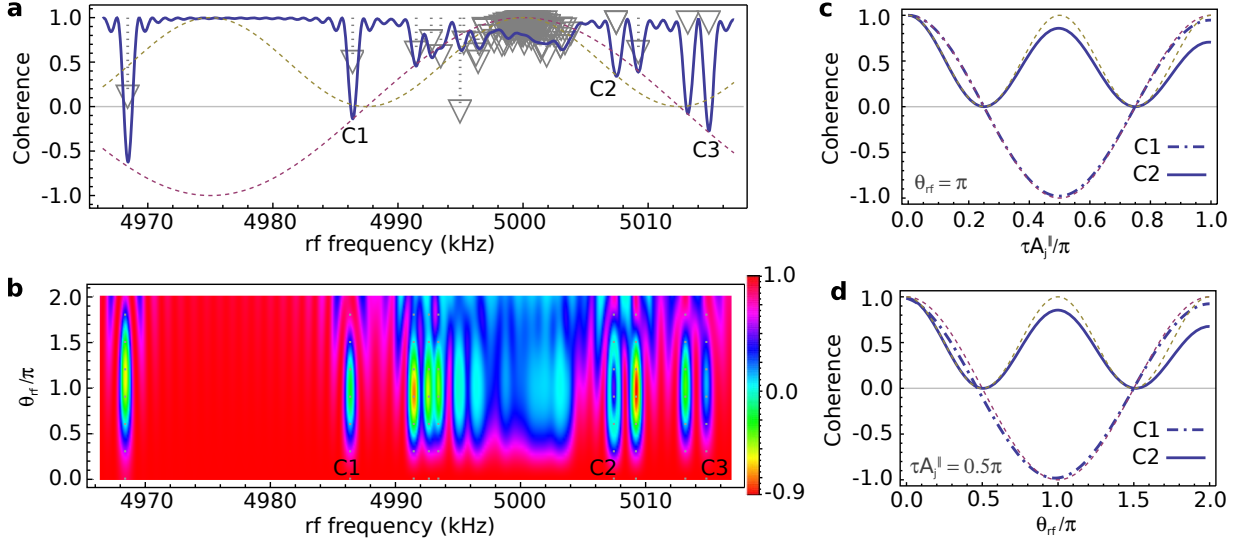


Figure 2: **Coherence signals of delayed entanglement echo by DD.** **a**, Coherence dips of NV electron qubit by using the electron spin levels $m_s = 0, 1$ for the interaction time $\tau = 10 \mu\text{s}$ and DD protected rf driving with single-spin rotation angle $\theta_{\text{rf}} = \pi$. The dashed lines shows the coherence signal $L^p(\omega_{\text{rf}} - \omega_{13\text{C}}, \theta_{\text{rf}})$ for one ($p = 1$) and two ($p = 2$) spins. **b**, As in **a** but changing θ_{rf} and transferring the NV electron qubit to the levels $m_s = \pm 1$ for the interaction windows with $\tau = 13 \mu\text{s}$. **c, d**, Coherence oscillations when changing τ and θ_{rf} using the scheme in **b**. The arrows (with the length proportional to A_j^\perp) in **a** and the vertical dotted lines in **b** show the precession frequencies ω_j (bare Larmor frequency $\omega_{13\text{C}} = 2\pi \times 5 \text{ MHz}$).

θ_{rf} will generate entanglement with the target and lead to an observable loss of coherence in the electron spin due to entanglement with the target nucleus. Additionally, more than one nuclear spins can be addressed in the same delay window by using rf driving with different

frequencies.

We will describe two strategies to achieve selective nuclear spin control in the delay window. In the first one we use DD techniques to suppress electron-nuclear interactions for protection of both the NV electron coherence

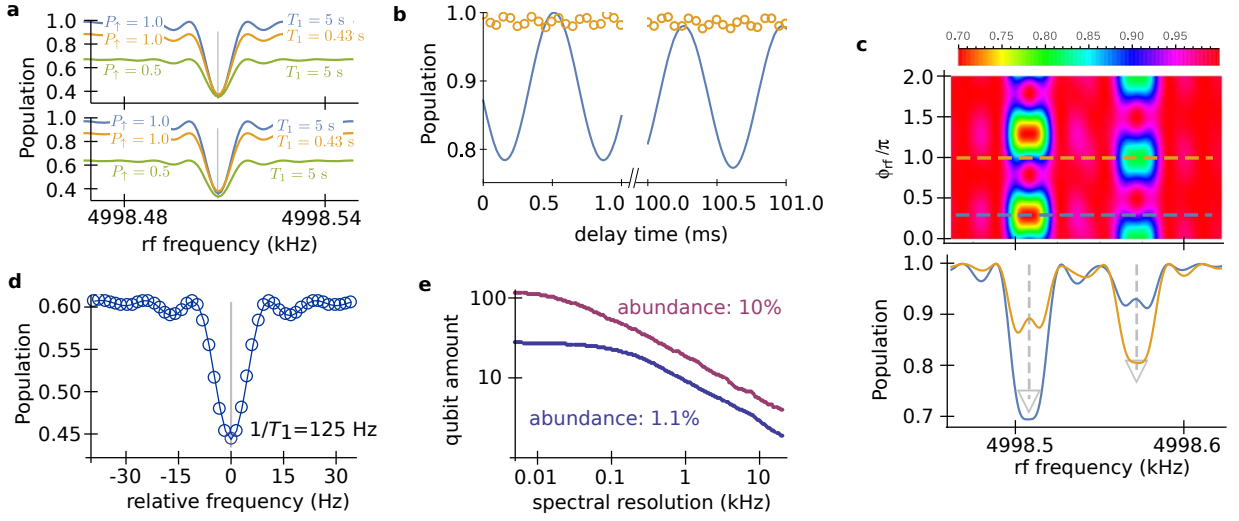


Figure 3: **Delayed entanglement echo by using a nuclear memory qubit.** **a**, Signal dips when addressing to a single distant ^{13}C nuclear spin ≈ 2.2 nm away from the NV centre by storing the qubit state in a ^{13}C (upper panel) or in the intrinsic ^{14}N (lower panel) memory qubit during the delay windows, for $t_{\text{rf}} = 100$ ms, $\tau = 100$ μs , and various low-temperature electron spin relaxation times T_1 and initial populations P_{\uparrow} of the memory qubit state $|\uparrow\rangle$. **b**, Population modulation (solid line) caused by two interacting ^{13}C nuclei in a C-C bond ~ 1.5 nm away from the NV centre with $\tau = 200$ μs and a ^{14}N memory. Application of LG decoupling suppresses nuclear dipolar interactions and hence the modulation (circles). **c**, Signal patterns from two uncoupled distant ^{13}C spins (2.2 and 2.3 nm away from the NV centre) when using a ^{14}N memory qubit and DD to protect the interaction windows of duration $\tau = 500$ μs (see Supplementary Information for the method). Lower panel shows the cross-sectional plots of upper panel (dashed lines) when the initial rf phases ϕ_{rf} match the azimuthal angles of addressed nuclear spins. **d**, Room-temperature signal of one proton spin placed 4 nm away from the NV centre using a ^{13}C memory qubit and optical illumination during the delay window (see Supplementary Information). With the rf driving of $t_{\text{rf}} \approx 10T_1$, the line-width of the signal is well beyond the limit set by electron spin relaxation time $1/T_1$. One major reason of the reduction of signal contrast is the leakage out from the electron qubit to another electron spin triplet level. **e**, Log-log plot of the average number of individual ^{13}C register qubits with $A_j^{\parallel} > 4$ kHz and A_j^{\parallel} different from other spins by amounts larger than the spectral resolution, by averaging over 1000 samples. A magnetic field is used for the bare Larmor frequency $\omega_{^{13}\text{C}} = 2\pi \times 5$ MHz. In **a,d,c**, $\theta_{\text{rf}} = \pi$, and $\theta_{\text{rf}} = 0$ in **b**. In **a,b**, the electron qubit state $|\downarrow_e\rangle = |0\rangle$ is transferred to $|\downarrow_e\rangle = |-1\rangle$ during the interaction windows.

and the rf nuclear spin control (Fig. 1e). Consider an NV centre in a diamond sample with natural ^{13}C abundance (1.1%) and initialise the NV-center in the equally weighted superposition state $|\psi_e\rangle$. Then the population signal $P = (1 + L)/2$ is directly related to the observable of NV electron coherence², $L = |\langle \downarrow_e | \psi_e \rangle \langle \psi_e | \uparrow_e \rangle|$. Fig. 2a,b shows the coherence when scanning the frequency of an rf-pulse with length $t_{\text{rf}} \approx 1$ ms in the delay window protected by 100-pulse Carr-Purcell (CP) sequences¹⁴. When the rf frequency matches one of the nuclear precession frequencies $\omega_j = \omega_{^{13}\text{C}} - A_j^{\parallel}/2$ under strong magnetic fields (with $\omega_{^{13}\text{C}}$ denoting the bare Larmor frequency of ^{13}C), we observe a coherence $L = L(A_j^{\parallel}, \theta_{\text{rf}})$ where the single spin contribution $L(A_j^{\parallel}, \theta_{\text{rf}}) = [(1 - \cos \theta_{\text{rf}}) \cos(2\eta A_j^{\parallel} \tau) + 1 + \cos \theta_{\text{rf}}]/2$ (see Supplementary Information). When there are p spins with the same ω_j , the coherence signal becomes $L = [L(A_j^{\parallel}, \theta_{\text{rf}})]^p$. The one-to-one correspondence between L and ω_j (see the dashed lines on Fig. 2 where $p = 1$ for C1 and C3 and $p = 2$ for C2) and the coherence patterns (see Fig. 2c,d) easily identifies the number of nuclear spins in a dip, even when they are not resolved in the spectrum.

Note that the signal is strong even when $A_j^{\perp} = 0$, which contrasts previous methods^{2-4,20-22} requiring relatively large A_j^{\perp} .

We can enhance the interaction and signal by transferring the electronic state $|\downarrow_e\rangle = |0\rangle$ to $|\downarrow_e\rangle = |-1\rangle$ during the interaction windows $[(t_1, t_2)$ and (t_5, t_6) in Fig. 1], as shown in Fig. 2b. Fig. 2b also shows that changing the rotation angle θ_{rf} does not affect the locations of signal dips, demonstrating an intrinsic robustness of our method in nuclear spin detection.

Alternatively, during the delay window we may store the electron spin state in a long-lived nuclear spin (see Fig. 1f). In Fig. 3a, we show the NV electron spin population signal when it addresses an isolated ^{13}C spin, by using an initially polarised memory qubit (see Methods). Because the electron spin is polarised to $m_s = +1$ during the delay window after a SWAP gate (see Supplementary Information), it is not necessary to protect electron coherence. Additionally the shifts of the nuclear spin precession frequencies (now $\omega_j = \omega_{^{13}\text{C}} - A_j^{\parallel}$ under strong magnetic fields) are larger than those achieved by the method described earlier or by DD^{2-4,20,21}. The electron spin relaxation creates magnetic noise on the nuclear

spins and can reduce the signal contrast¹. However, at low temperatures, the relaxation time T_1 of NV electron spin can reach minutes²³. When $T_1 \gg t_{\text{rf}}$ the effects of electron spin relaxation can be neglected. Additionally, we can protect the memory qubit against the electron-relaxation noise for example by strong driving¹. Even for unpolarised memory qubit, the signal contrast is still large, showing that our method is insensitive to initialisation error of the qubit memory (Fig. 3a).

Structural information of coupled spin clusters can also be observed by our method. The dynamics of two coupled spins under a strong magnetic field is characterised by the dipolar coupling strength $d_{j,k}$ and the difference $\delta_{j,k} = A_j^{\parallel} - A_k^{\parallel}$ between the hyperfine components²⁴. A pair of ^{13}C spins with $d_{j,k} \approx \delta_{j,k}$ close to the NV centre can modulate the NV coherence^{24,25}, in the absence of rf control as shown in Fig. 3b. Spin pairs with $|\delta_{j,k}| \gg |d_{j,k}|$ or $|\delta_{j,k}| \ll |d_{j,k}|$, which could be useful quantum resources, were regarded as unobservable, because they form stable pseudo-spins which have negligible effects on electron coherence²⁴. But using our method, we can detect, identify, and control those spin pairs close to the NV centre (see Supplementary Information for details).

To address and control nuclear spins individually in a coupled cluster the internuclear dipolar coupling needs to be suppressed. Internuclear interactions also reduce the Hahn-echo electron coherence times and, hence, the achievable interaction times τ (available values $\tau \sim 0.5$ ms for natural abundance of ^{13}C and can be increased using lower abundance)^{26,27}. To solve the problem of spin interactions, we use the Lee-Goldburg (LG) off-resonance decoupling¹⁴ (see Methods). When the LG decoupling field is tuned such that $\sqrt{2}\Delta_{\text{LG}} \gg d_{jk}$, the dipolar coupling between nuclear spins are suppressed^{17,21}, giving rise to the effective interaction Hamiltonian $H_{\text{int}} \approx \eta \sum_j A_j^{\parallel} \cos \gamma_j \sigma_z \tilde{I}_j^z / \sqrt{3}$ with \tilde{I}_j^z the nuclear spin operators projected along effective rotating axes (see Supplementary Information). Fig. 3b demonstrates the effect of LG decoupling with $\Delta_{\text{LG}} = 2\pi \times 20$ kHz. The suppression of the internuclear interactions allows us to achieve much longer interaction times τ and rf pulse lengths t_{rf} for single spin addressing. The improved spectral resolution $\sim 1/t_{\text{rf}}$ leads to an increase of the number of individually addressable spins (see Fig. 3e).

In the case that there are other significant decoherence sources that are acting on the NV electron spin, our method can be combined with DD to further protect the NV coherence. Applying CP sequences with an inter π -pulse interval π/ω_{DD} during the interaction windows, noise with frequencies slower than ω_{DD} is suppressed, and at the same time the electron spin couples to nuclear spins through the interactions $2\eta/(k\pi)A_j^{\perp}\sigma_z I_j^{\varphi_j}$ when the nuclear precession frequencies ω_j are resonant with $k\omega_{\text{DD}}$ (k being odd integers)^{4,20,21}. The nuclear spin operators $I_j^{\varphi_j} = I_j^x \cos \varphi_j + I_j^y \sin \varphi_j$ depends on the azimuthal angles φ_j of nuclear spins relative to the

magnetic field direction. Nuclear spins unresolvable by the CP sequences may nevertheless have different precession rates. To ensure the same effective Hamiltonian during the interaction windows, we apply a two-pulse CP sequence on the nuclear spins during the delay window to remove this inhomogeneity. Then adding a weak rf drive during the delay window allows us to address the target spins with high spectral resolutions. Additionally, the scheme allows us to measure the spin directions φ_j , because the rf driving has negligible effects when the azimuthal angle (phase) of rf control $\phi_{\text{rf}} = \varphi_j$ or $\varphi_j + \pi$ (see Fig. 3c and Supplementary Information). Note that we can combine LG decoupling with DD using recently proposed protocols^{21,28}.

Our method allows to improve the spectral resolution beyond the limit set by the room-temperature electron T_1 , using optical illumination that has been demonstrated to prolong the room-temperature coherence time of nuclear spin memory over one second (~ 267 times of T_1)¹. To demonstrate the idea, we simulate the application of optical illumination and rf driving during the delay window to detect a proton spin placed 4 nm away from the NV centre with interaction times $\tau = 100 \mu\text{s}$. A delay time $t_{\text{rf}} \approx 80$ ms used in Fig. 3d already provide enough frequency resolution to detect chemical shift of ~ 1 ppm for the applied magnetic field $B_z \approx 0.467$ T. We can apply LG decoupling when there are more target spins and internuclear interactions. In addition, we can use DD to protect the interaction windows from noise for extending the interaction time τ . Electron spin coherence time of shallow NV centre has reported values of ~ 1 ms using continuous DD (spin lock)¹⁶.

In summary, we have proposed a method to address and control nuclear spins which were regarded as unresolvable. The method significantly increases the ability of detection and coherence control of nuclear spins and has applications in quantum information processing as well as analysis of chemical shifts and dynamics of spin clusters. The method is general and can be applied to other electron-nuclear spin systems^{29,30}.

Methods

The memory nuclear spin qubit can be initialized by swapping the initialized NV electron qubit state to the memory spin or by using dynamical nuclear polarization. Details on the swap operations are presented in Supplementary Information.

The LG decoupling field^{17,21,31} can remain turned on for the entire duration of our protocol, including NV electron spin initialization and readout, because the frequency of rf decoupling field is far off-resonance to the transition frequencies of the NV electron spin. This allows for the rf decoupling field to be applied by external coils and resonators to avoid possible heating on the diamond sample. The LG decoupling with $\Delta_{\text{LG}} = 2\pi \times 20$ kHz requires a rf field's amplitude to be much smaller than the values of ~ 0.1 T in the control fields reported in refs. 32,33.

- ¹ Maurer, P. C. *et al.* Room-temperature quantum bit memory exceeding one second. *Science* **336**, 1283-1286 (2012).
- ² Zhao, N. *et al.* Sensing single remote nuclear spins. *Nature Nanotech.* **7**, 657-662 (2012).
- ³ Kolkowitz, S., Unterreithmeier, Q. P., Bennett, S. D. & Lukin, M. D. Sensing distant nuclear spins with a single electron spin. *Phys. Rev. Lett.* **109**, 137601 (2012).
- ⁴ Taminiau, T. H. *et al.* Detection and control of individual nuclear spins using a weakly coupled electron spin. *Phys. Rev. Lett.* **109**, 137602 (2012).
- ⁵ Liu, G.-Q., Po, H. C., Du, J., Liu, R.-B. & Pan, X.-Y. Noise-resilient quantum evolution steered by dynamical decoupling. *Nature Commun.* **4**, 2254 (2013).
- ⁶ Taminiau, T. H., Cramer, J., van der Sar, T., Dobrovitski, V. V. & Hanson, R. Universal control and error correction in multi-qubit spin registers in diamond. *Nature Nanotech.* **9**, 171-176 (2014).
- ⁷ Waldherr G. *et al.* Quantum error correction in a solid-state hybrid spin register. *Nature* **506**, 204-207 (2014).
- ⁸ London, P. *et al.* Detecting and polarizing nuclear spins with nuclear double resonance on a single electron spin. *Phys. Rev. Lett.* **111**, 067601 (2013).
- ⁹ Schirhagl, R., Chang, K., Loretz, M. & Degen, C. L. Nitrogen-vacancy centers in diamond: nanoscale sensors for physics and biology. *Annu. Rev. Phys. Chem.* **65**, 83-105 (2014).
- ¹⁰ Laraoui, A. *et al.* High-resolution correlation spectroscopy of ¹³C spins near a nitrogen-vacancy centre in diamond. *Nature Commun.* **4**, 1651 (2013).
- ¹¹ Doherty, M. W. *et al.* The nitrogen-vacancy colour centre in diamond. *Phys. Rep.* **528**, 1-45 (2013).
- ¹² Loretz, M. *et al.* Spurious harmonic response of multipulse quantum sensing sequences. *Phys. Rev. X* **5**, 021009 (2015).
- ¹³ Zhong, M. *et al.* Optically addressable nuclear spins in a solid with a six-hour coherence time. *Nature* **517**, 177-180 (2015).
- ¹⁴ Mehring, M. *Principle of High Resolution NMR in Solids* (Springer, New York, 1983).
- ¹⁵ Müller, C. *et al.* Nuclear magnetic resonance spectroscopy with single spin sensitivity. *Nature Commun.* **5**, 4703 (2014).
- ¹⁶ Lovchinsky, I. *et al.* Nuclear magnetic resonance detection and spectroscopy of single proteins using quantum logic. *Science* **351**, 836-841 (2016).
- ¹⁷ Cai, J., Retzker, A., Jelezko, F. & Plenio, M. B. A large-scale quantum simulator on a diamond surface at room temperature. *Nature Phys.* **9**, 168-173 (2013).
- ¹⁸ Yang, W., Wang, Z.-Y. & Liu, R.-B. Preserving qubit coherence by dynamical decoupling. *Front. Phys.* **6**, 2-14 (2011).
- ¹⁹ Cai, J.-M., Jelezko, F., Plenio, M. B. & Retzker, A. Diamond based single molecule magnetic resonance spectroscopy. *New J. Phys.* **15**, 013020 (2013).
- ²⁰ Casanova, J., Wang, Z.-Y., Haase, J. F. & Plenio, M. B. Robust dynamical decoupling sequences for individual nuclear-spin addressing. *Phys. Rev. A* **92**, 042304 (2015).
- ²¹ Wang, Z.-Y., Haase, J. F., Casanova, J. & Plenio, M. B. Positioning nuclear spins in interacting clusters for quantum technologies and bio-imaging. Preprint at <http://arxiv.org/abs/1510.02811> (2015).
- ²² Ma, W.-L. & Liu, R.-B. Scheme of angstrom-resolution magnetic resonance imaging of single molecules via wavefunction fingerprints of nuclear spins. Preprint at <http://arxiv.org/abs/1510.04081> (2016).
- ²³ Yang, S. *et al.* High fidelity transfer and storage of photon states in a single nuclear spin. Preprint at <http://arxiv.org/abs/1511.04939> (2015).
- ²⁴ Zhao, N., Hu, J.-L., Ho, S.-W., Wan, J. T. K. & Liu, R.-B. Atomic-scale magnetometry of distant nuclear spin clusters via nitrogen-vacancy spin in diamond. *Nature Nanotech.* **6**, 242-246 (2011).
- ²⁵ Shi, F. Z. *et al.* Sensing and atomic-scale structure analysis of single nuclear-spin clusters in diamond. *Nature Phys.* **10**, 21-25 (2014).
- ²⁶ Cramer, J. *et al.* Repeated quantum error correction on a continuously encoded qubit by real-time feedback. Preprint at <http://arxiv.org/abs/1508.01388> (2015).
- ²⁷ Zhao, N., Ho, S.-W. & Liu, R.-B. Decoherence and dynamical decoupling control of nitrogen vacancy center electron spins in nuclear spin baths. *Phys. Rev. B* **85**, 115303 (2012).
- ²⁸ Casanova, J., Wang, Z.-Y. & Plenio, M. B. Noise-resilient quantum computing with a nitrogen-vacancy center and nuclear spins. Preprint at <http://arxiv.org/abs/1602.06862> (2016).
- ²⁹ Widmann, M. *et al.* Coherent control of single spins in silicon carbide at room temperature. *Nature Mater.* **14**, 164-168 (2015).
- ³⁰ Dehollain, J. P. *et al.* Bell's inequality violation with spins in silicon. *Nature Nanotech.* **11**, 242-246 (2016).
- ³¹ Lee, M. & Goldburg, W. I. Nuclear-magnetic-resonance line narrowing by a rotating rf field. *Phys. Rev.* **140**, A1261 (1965).
- ³² Michal, C. A., Hastings, S. P. & Lee, L. H. Two-photon Lee-Goldburg nuclear magnetic resonance: Simultaneous homonuclear decoupling and signal acquisition. *J. Chem. Phys.* **128**, 052301 (2008).
- ³³ Fuchs, G. D., Dobrovitski, V. V., Toyli, D. M., Heremans, F. J. & Awschalom, D. D. Gigahertz dynamics of a strongly driven single quantum spin. *Science* **326**, 1520-1522 (2009).

Acknowledgements

This work was supported by the Alexander von Humboldt Foundation, the ERC Synergy grant BioQ, the EU projects DIADEMS, SIQS and EQUAM as well as the DFG via the SFB TRR/21. We thank Thomas Uden and Fedor Jelezko for discussions. Simulations were performed on the computational resource bwUniCluster funded by the Ministry of Science, Research and the Arts Baden-Württemberg and the Universities of the State of Baden-Württemberg, Germany, within the framework program bwHPC.

Author contributions

Z.Y.W., J.C., and M.B.P. conceived the idea. Z.Y.W. carried out the simulations and analytical work with input from J.C. and M.B.P. All authors discussed extensively on the results and contributed to the manuscript.

Additional information

The authors declare no competing financial interests. Correspondence and requests for materials should be addressed to Z.Y.W. (zhenyu3cn@gmail.com), J.C. (jcas-anovamar@gmail.com), or M.B.P. (martin.plenio@uni-ulm.de).

Supplementary Information for “Delayed entanglement echo for individual control of a large number of nuclear spins”

Contents

References	5
I. Hamiltonian of NV centre and nuclear spins	1
II. Spin addressing by dynamical decoupling	2
A. Effective interaction Hamiltonians under dynamical decoupling	2
B. Shortcomings of spin addressing by dynamical decoupling	3
III. Storage of electron states to a memory qubit	5
A. Storage to the intrinsic nitrogen spin	5
B. Storage to carbon-13 memory qubits	6
IV. Signals of delayed entanglement echo	7
A. Single spins	7
B. Coupled spin pairs	7
V. Combining the interaction windows with dynamical decoupling	9
VI. Simulation details	9
References	11

I. HAMILTONIAN OF NV CENTRE AND NUCLEAR SPINS

Under a magnetic field $\mathbf{B} = B_z \hat{z}$ along the NV symmetry axis, the Hamiltonian of NV centre electron spin and its nuclear environment reads ($\hbar = 1$)

$$H = H_{\text{NV}} + H_{\text{nZ}} + H_{\text{hf}} + H_{\text{nn}}. \quad (\text{S1})$$

Here $H_{\text{NV}} = DS_z^2 - \gamma_e B_z S_z$ is the electron spin Hamiltonian with the spin operator $S_z = \sum_{m_s=\pm 1,0} m_s |m_s\rangle \langle m_s|$, the ground state zero field splitting $D \approx 2\pi \times 2.87$ GHz, and $\gamma_e = -2\pi \times 2.8$ MHz/G the electron spin gyromagnetic ratio^{S1}. The nuclear Zeeman Hamiltonian $H_{\text{nZ}} = -\sum_j \gamma_j \mathbf{B} \cdot \mathbf{I}_j$, where γ_j is the nuclear gyromagnetic ratio and \mathbf{I}_j is the spin operator for the j -th nuclear spin. The dipole-dipole interactions between nuclear spins are

$$H_{\text{nn}} = \sum_{j>k} \frac{\mu_0}{4\pi} \frac{\gamma_j \gamma_k}{|\mathbf{r}_{j,k}|^3} \left[\mathbf{I}_j \cdot \mathbf{I}_k - \frac{3(\mathbf{I}_j \cdot \mathbf{r}_{j,k})(\mathbf{r}_{j,k} \cdot \mathbf{I}_k)}{|\mathbf{r}_{j,k}|^2} \right], \quad (\text{S2})$$

with μ_0 being the vacuum permeability, $\mathbf{r}_{j,k} = \mathbf{r}_j - \mathbf{r}_k$ the difference between the k -th and j -th nuclear positions. Typically the electron-nuclear flip-flop terms in the hyperfine interaction H_{hf} are suppressed by the large energy mismatch between electron and nuclear spins, giving $H_{\text{hf}} = S_z \sum_j \mathbf{A}_j \cdot \mathbf{I}_j$ under the secular approximation. However, for strong hyperfine interactions the virtual flips of the electron spin could cause observable effects, an aspect that we will discuss later (see Sec. III A). For nuclear spins not too close to the NV centre, the hyperfine interaction takes the dipolar form and the hyperfine field

$$\mathbf{A}_j = \frac{\mu_0}{4\pi} \frac{\gamma_e \gamma_j}{|\mathbf{r}_j|^3} \left(\hat{z} - \frac{3\hat{z} \cdot \mathbf{r}_j \mathbf{r}_j}{|\mathbf{r}_j|^2} \right). \quad (\text{S3})$$

Because the total Hamiltonian under secular approximation commutes with H_{NV} , we simply remove it by going to the rotating frame with respect to H_{NV} . We choose two of the three triplet states as the qubit basis states for the NV electron spin. The Hamiltonian becomes

$$H_\eta = \eta \sigma_z \sum_j \mathbf{A}_j \cdot \mathbf{I}_j + H_{\text{n},\eta} + H_{\text{nn}}. \quad (\text{S4})$$

In the manifold of the electron spin levels $|\uparrow_e\rangle = | + 1 \rangle$ and $|\downarrow_e\rangle = | 0 \rangle$, we have the coupling constant $\eta = 1/2$, while for the electron spin levels $|\uparrow_e\rangle = | + 1 \rangle$ and $|\downarrow_e\rangle = | - 1 \rangle$, $\eta = 1$. The nuclear Hamiltonian describing nuclear precession reads

$$H_{n,\eta} = - \sum_j (\gamma_j \mathbf{B} - c_\eta \mathbf{A}_j) \cdot \mathbf{I}_j \equiv -\omega_j \hat{\omega}_j \cdot \mathbf{I}_j, \quad (\text{S5})$$

where the unit vectors $\hat{\omega}_j$ denote the directions of $\gamma_j \mathbf{B} - c_\eta \mathbf{A}_j$ with $c_\eta = 1/2$ when $\eta = 1/2$ and $c_\eta = 0$ if $\eta = 1$. For the case of H_1 ($\eta = 1$), the electron-nuclear coupling is stronger and the nuclear precession frequencies $\omega_j = \gamma_j B_z$ are the bare nuclear Larmor frequencies. While for the case of $H_{\frac{1}{2}}$ ($\eta = 1/2$), the electron-nuclear coupling is weaker and the precession frequencies $\omega_j = |\gamma_j \mathbf{B} - \frac{1}{2} \mathbf{A}_j|$ are shifted by the hyperfine field at the positions of the nuclear spins.

In the rotating frame of nuclear spin precession $H_{n,\eta}$, the interaction Hamiltonian $\eta \sigma_z \sum_j \mathbf{A}_j \cdot \mathbf{I}_j$ becomes^{S2}

$$H_{\text{int}} = \eta \sigma_z \sum_j [\mathbf{A}_j^x \cos(\omega_j t) + \mathbf{A}_j^y \sin(\omega_j t) + \mathbf{A}_j^z] \cdot \mathbf{I}_j, \quad (\text{S6})$$

with

$$\mathbf{A}_j^x \equiv \mathbf{A}_j - \mathbf{A}_j^z, \quad (\text{S7})$$

$$\mathbf{A}_j^y \equiv \hat{\omega}_j \times \mathbf{A}_j, \quad (\text{S8})$$

$$\mathbf{A}_j^z \equiv \mathbf{A}_j \cdot \hat{\omega}_j \hat{\omega}_j. \quad (\text{S9})$$

The hyperfine components have the strengths $|\mathbf{A}_j^x| = |\mathbf{A}_j^y| = A_j^\perp$ and $|\mathbf{A}_j^z| = A_j^\parallel$. The time-dependent terms in Eq. (S6) do not commute with the nuclear precession $H_{n,\eta}$.

Under a strong magnetic field $B_z \gg A_j^\perp$, $\hat{\omega}_j \approx \hat{z}$. The nuclear spin flips are suppressed, giving

$$H_{\text{int}} \approx \eta \sigma_z \sum_j \mathbf{A}_j^z \cdot \mathbf{I}_j = \eta \sigma_z \sum_j A_j^\parallel I_j^z. \quad (\text{S10})$$

If we apply Lee-Goldburg (LG) off-resonance control^{S3}, we can achieve similar Hamiltonians^{S4,S5}

$$H_{\text{int}}^{\text{LG}} \approx \eta \sigma_z \sum_j A_j^\parallel \cos \gamma_j \tilde{I}_j^z, \quad (\text{S11})$$

where $\tilde{I}_j^z = \hat{\nu}_j \cdot \mathbf{I}_j$ with $\hat{\nu}_j$ the unit vector denoting the nuclear precession in the frame of LG control. The projection factor $\cos \gamma_j = \hat{\omega}_j \cdot \hat{\nu}_j \approx 1/\sqrt{3}$.

The interaction Hamiltonian Eq. (S10) commutes with the nuclear precession. Similarly, Eq. (S11) commutes with the nuclear precession around $\hat{\nu}_j$ in the frame of LG control. Combined with the delay entanglement control described in the main text, we can keep only terms on the target spins in H_{int} or $H_{\text{int}}^{\text{LG}}$. The effective electron-nuclear interactions by delay entanglement control do not broaden the nuclear precession frequencies for addressing.

II. SPIN ADDRESSING BY DYNAMICAL DECOUPLING

A. Effective interaction Hamiltonians under dynamical decoupling

Nuclear spins can be addressed by dynamical decoupling (DD)^{S2,S4,S6-S10}. The DD pulses flip the NV electron qubit. After application of n π pulses, $\sigma_z \rightarrow F(t)\sigma_z$ with the modulation function $F(t) = (-1)^n$. We consider periodic sequences with $F(t) = F(t + 2\pi/\omega_{\text{DD}})$ in this work. The interaction Hamiltonian Eq. (S6) becomes

$$H_{\text{int}} = \eta F(t) \sigma_z \sum_j [\mathbf{A}_j^x \cos(\omega_j t) + \mathbf{A}_j^y \sin(\omega_j t) + \mathbf{A}_j^z] \cdot \mathbf{I}_j. \quad (\text{S12})$$

This instantaneous-pulse control changes the electron-nuclear dynamics^{S7,S11,S12}. To get insight on nuclear spin sensing by DD pulse sequences, we expand the modulation function in a Fourier series,

$$F(t) = \sum_{k \geq 1} [f_k^s \cos(k\omega_{\text{DD}}t) + f_k^a \sin(k\omega_{\text{DD}}t)],$$

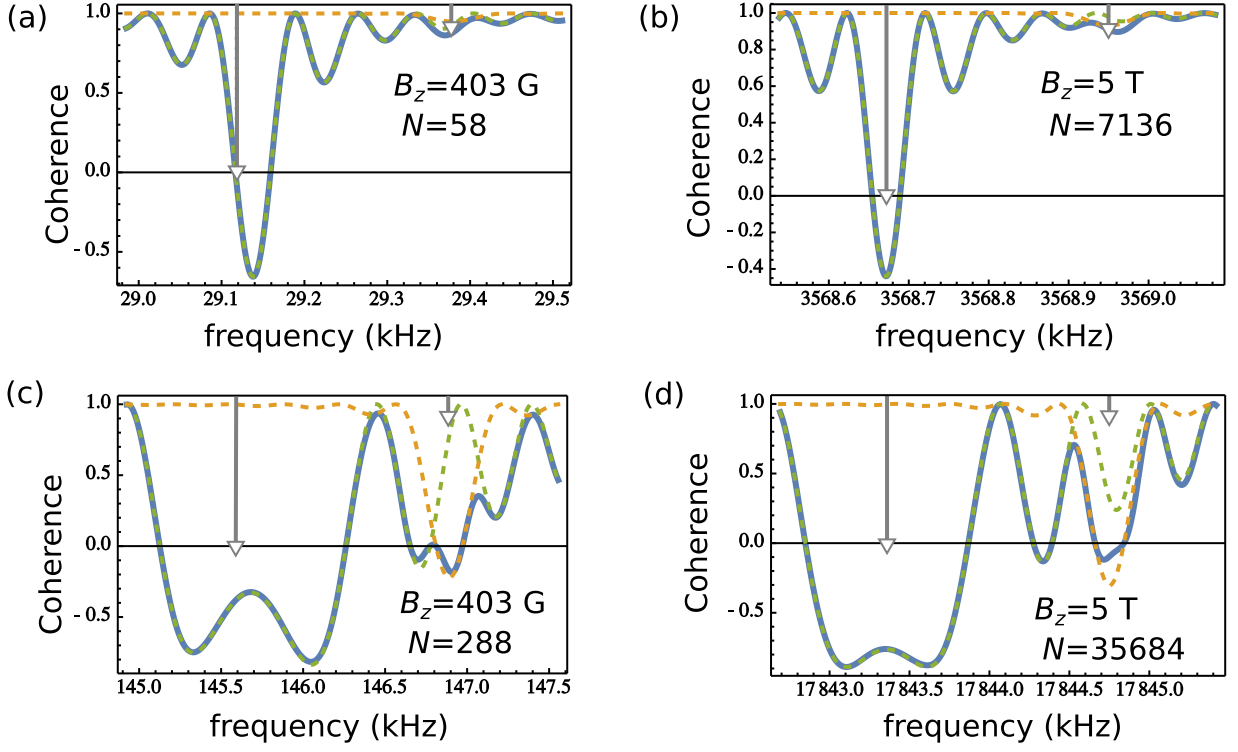


Figure S1: **Coherence signals obtained by CP sequences.** Coherence of NV electron spin (blue solid line) as a function of DD frequency $\omega_{\text{DD}} = \pi/\tau_{\text{CP}}$ (with τ_{CP} the pulse intervals of CP sequences), under the control of N -pulse CP sequences at a magnetic field B_z . The CP sequences have durations of ~ 1 ms using the pulse numbers and magnetic fields indicated on the figures. The green and yellow dashed lines are the signals of single spins. The arrows indicate the frequencies ω_j/k_{DD} with the lengths proportional to A_j^\perp . The signals of resonances at $k_{\text{DD}} = 15$ in (a) and (b) are dominated by the nuclear spin with a strong A_j^\perp . While in (c) and (d), increasing the interactions by using a smaller $k_{\text{DD}} = 3$ also increases the interference from the spin with a strong A_j^\perp , prohibiting the spin addressing on the nuclear spin with a weaker A_j^\perp . In (b) and (d), the number of pulses increases under a stronger magnetic field, compared with the cases in (a) and (c).

using that DD pulses have been designed to remove static noise and hence there is no static term in the Fourier series. For periodic symmetric sequences $f_k^a = 0$. The frequency ω_{DD} characterises the flipping rate of the NV electron qubit. For example, for the traditional Carr-Purcell (CP) sequence^{S13} and its variations^{S14-S16} having a time interval τ_{CP} between successive π pulses, $\omega_{\text{DD}} = \pi/\tau_{\text{CP}}$, $f_k^s = 4(k\pi)^{-1} \sin(k\pi/2)$, and $f_k^a = 0$. The expansion coefficients can be tuned by adaptive XY (AXY) sequences^{S2}.

A nuclear spin with the precession frequency ω_n can be addressed by resonance to the k_{DD} harmonic of the driving rate, that is, $\omega_n = k_{\text{DD}}\omega_{\text{DD}}$. With the additional conditions (with $j \neq n$) $|\gamma_j B_z| \gg k_{\text{DD}}|A_j|$ and

$$|\omega_n - \omega_j| \gg |f_{k_{\text{DD}}} A_j^\perp|, \quad (\text{S13})$$

we have single spin addressing under periodic symmetric sequences $H_{\text{int}} \approx (\eta/2)f_{k_{\text{DD}}}^s A_j^\perp \sigma_z I_j^x$ ^{S2}. Similar addressing Hamiltonians ($H_{\text{int}}^{\text{LG}} \propto \sigma_z \tilde{I}_j^x$ with \tilde{I}_j^x a spin operator projected perpendicular to \hat{v}_j) can be achieved under LG control^{S4,S17}.

Nuclear spins can also be addressed by continuous DD^{S9}. In the rotating frame of a constant microwave driving $\Omega_e \sigma_x/2$ with the Rabi frequency Ω_e (the frequency of nuclear spin precession in the spin-lock frame), the Pauli operator of NV electron qubit transforms as $\sigma_z \rightarrow \sigma_z \cos(\Omega_e t) + \sigma_y \sin(\Omega_e t)$. The driving rate of the electron spin is $\omega_{\text{DD}} = \Omega_e$. When Ω_e is on-resonance to the nuclear spin precession frequency ω_j , that is, $\Omega_e = \omega_j$, we have the addressing Hamiltonian $H_{\text{int}} \approx (\eta/2)A_j^\perp (\sigma_z I_j^x + \sigma_y I_j^y)$ when $|\gamma_j B_z| \gg |A_j|$ and $|\omega_n - \omega_j| \gg A_j^\perp$ for $j \neq n$.

B. Shortcomings of spin addressing by dynamical decoupling

The addressing by DD has a number of shortcomings that we are going to discuss in the following.

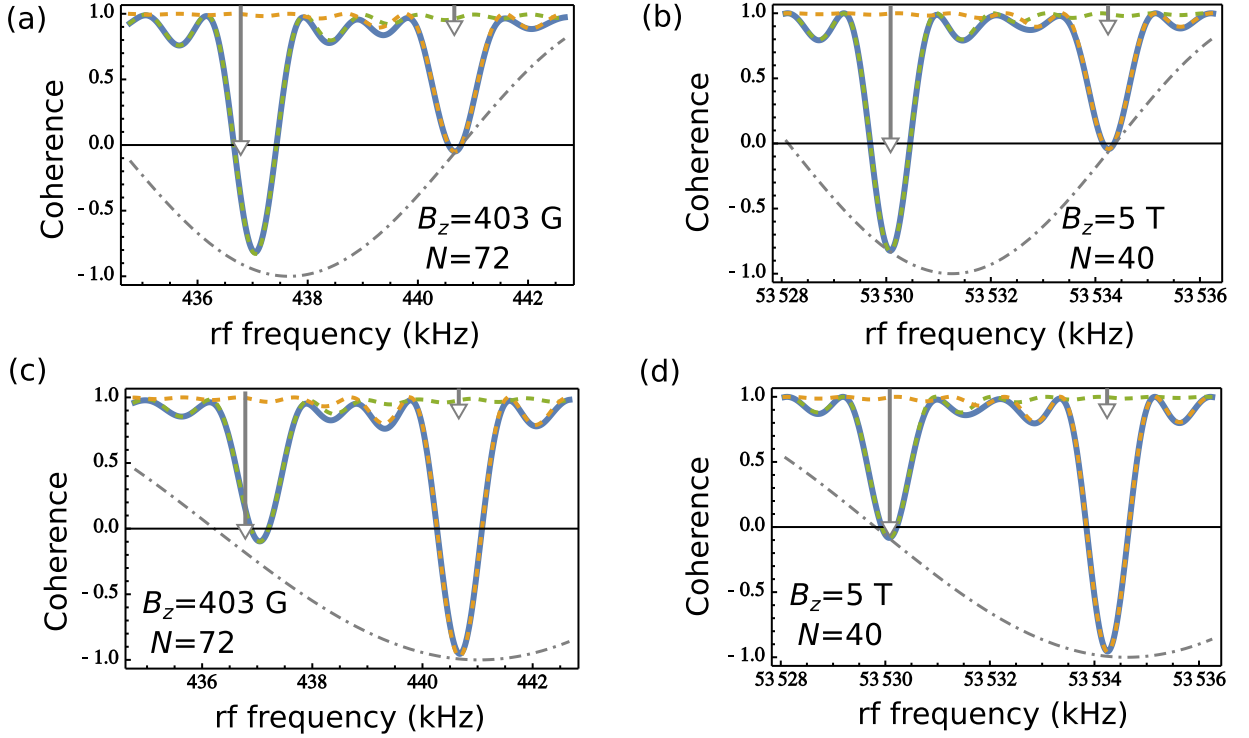


Figure S2: **Coherence signals obtained by delayed entanglement echoes.** Coherence of NV electron spin (blue solid line) as a function of the frequency ω_{rf} of rf driving at the delay window, which the duration $t_{\text{rf}} \approx 1$ ms and $\theta_{\text{rf}} = \pi$. The pulse number N of CP sequences used to protect the delay window are indicated on the figures, as well as the magnetic field B_z . The green and yellow dashed lines are the signals of single spins. Each of the arrow located at the nuclear precession frequency ω_j has a length proportional to A_j^\perp . The interaction times $\tau = 20 \mu\text{s}$ for (a) and (b), while a shorter $\tau = 13 \mu\text{s}$ for (c) and (d). Dash-dotted lines are the curve $\cos[4\tau(\omega_{\text{rf}} - \omega_{13\text{C}})]$. The qubit levels $m_s = \pm 1$ are used at the interaction windows.

First, the interaction Hamiltonians achieved by DD do not commute with the nuclear precession. As a consequence, electron-nuclear interactions broaden the nuclear precession frequencies for addressing (see Figs. S1 (c) and (d)). We need the condition in Eq. (S13) for individual spin addressing. Reducing the effective interaction strengths between NV electron and nuclear spins improves a lot the spectral resonance by using higher harmonics $k_{\text{DD}} > 1$, by alternating the phase of Rabi driving^{S10}, or by using composite π pulses^{S2,S4,S18,S19}. But the reduced coupling also makes nuclear spins that are not strongly coupled hard to detect and control (see Figs. S1 (a) and (b)).

Second, because resonances can occur at different harmonic frequencies $k\omega_{\text{DD}}$, resonance lines from different harmonic branches can have overlaps and make critical ambiguities in detection and addressing^{S2,S7,S20}. The spurious resonances caused by realistic pulse width further complicate the situation, even making false identification of different nuclear species (e.g., ^{13}C and ^1H)^{S20}.

Third, the achievable rate ω_{DD} of DD sets an upper limit on the external magnetic field for spin addressing. A strong magnetic field is the requirement in detecting the chemical shift of nuclear spins^{S21} and in decoupling of the nuclear dipole-dipole interactions by rf control^{S3-S5}. In addition, the NV electron coherence can be protected easier under strong magnetic fields^{S22}. However, nuclear spin precession frequencies ω_j at strong magnetic fields can be significantly larger than the achievable rate ω_{DD} of DD control. For example, the pulse number 35684 required in Fig. S1 (d) could be too many in experiments. Using resonance branches with large k_{DD} can reduce the required control rate ω_{DD} , but it also reduces electron-nuclear coupling and narrows spectral bandwidths (in Fig. S1 (b) the coupling is too weak to detect the nuclear spin with a weak A_j^\perp and the bandwidth is about $\sim \omega_{13\text{C}}/k_{\text{DD}}$ for ^{13}C spins).

The delayed entanglement echo technique does not suffer from the above shortcomings (compare Fig. S2 with Fig. S1), and provide some additional advantages. First, it does not require both hyperfine components A_j^\parallel and A_j^\perp to be strong. Second, both the electron-nuclear coupling strengths before and after the delay window are not reduced. In addition, we can use the levels $m_s = \pm 1$ to double the interaction strength (changing $\eta = 1/2$ to $\eta = 1$), since the nuclear spins are addressed by the control in the delay window. In contrast, $\eta = 1/2$ is necessary during the whole protocol of spin addressing by standard DD, so that homonuclear spins feeling different hyperfine fields have different

precession frequencies. Third, our technique allows to simultaneously address more than one nuclear spin by applying rf driving fields at the frequencies of those spins during a delay window.

III. STORAGE OF ELECTRON STATES TO A MEMORY QUBIT

Here we present more details on storing the electron qubit states to a nuclear spin memory. During the swap operations, the NV electron qubit is working in the $m_s = 0, +1$ manifold. Storage of electron spin state can be realised by SWAP gates. A SWAP gate

$$\text{SWAP} = \sum_{m_s, m_n=0,1} |m_s m_n\rangle \langle m_n m_s| \quad (\text{S14})$$

swap the electron qubit states m_s and memory qubit states m_n . In the case that relaxations of the electron and nuclear memory qubit can be neglected during the delay window, we can also use iSWAP gate

$$\text{iSWAP} = \sum_{m_s, m_n=0,1} e^{i(m_s+m_n)^2 \pi/2} |m_s m_n\rangle \langle m_n m_s|, \quad (\text{S15})$$

which introduces a phase factor i when $m_s \neq m_n$. Without relaxations of the electron and nuclear memory qubit, the whole system including the environment and the memory qubit has the evolution during the delay window

$$U_{\text{delay}} = \sum_{m_s, m_n=0,1} |m_s m_n\rangle \langle m_s m_n| \otimes U_{m_s, m_n}, \quad (\text{S16})$$

where U_{m_s, m_n} are unitary evolution operators of the environment part. The effect of the iSWAP gates,

$$\text{iSWAP}^\dagger U_{\text{delay}} \text{iSWAP} = \sum_{m_s, m_n=0,1} |m_n m_s\rangle \langle m_n m_s| \otimes U_{m_s, m_n}, \quad (\text{S17})$$

is the same as using SWAP gates.

We use protected swap gates to suppress decoherence of the NV electron spin and unwanted electron-nuclear interactions during gate implementation. Using nuclear spin addressing by DD^{S2, S4, S11, S23} or the delayed entanglement echo presented in the main text, we implement the elementary decoherence-protected two qubit gates $u_{z\alpha} = \exp(i\frac{\pi}{4}\sigma_z I_\alpha)$ with $\alpha = x, y, z$ as well as single qubit gates for nuclear spins. Combining the gate $u_{z\alpha}$ with electron spin rotations, we achieve the gate $u_{\alpha\alpha} = \exp(i\frac{\pi}{4}\sigma_\alpha I_\alpha)$ [e.g., $u_{yy} = \exp(i\frac{\pi}{4}\sigma_x) u_{zy} \exp(-i\frac{\pi}{4}\sigma_x)$]. A swap gate is constructed by $u_{zz} u_{yy} u_{xx}$, where the three gates $u_{\alpha\alpha}$ commute, while $u_{yy} u_{xx}$ gives rise to the iSWAP gate.

A. Storage to the intrinsic nitrogen spin

Here we describe the details of implementation of SWAP gates between the electron qubit and the intrinsic nitrogen spin qubit. For simplicity, we consider ¹⁴N, which has 99.636% natural abundance and a spin $I = 1$. The Hamiltonian for the NV electron and the intrinsic nitrogen spins is

$$H_{\text{NV}} = DS_z^2 - \gamma_e B_z S_z + P I_z^2 - \gamma_N B_z I_z + A^\parallel S_z I_z + A^\perp (S_x I_x + S_y I_y), \quad (\text{S18})$$

where $\gamma_N = 2\pi \times 0.308$ kHz/G. We adopt the parameters for ¹⁴N in NV centres $A^\perp = -2\pi \times 2.62$ MHz, $A^\parallel = -2\pi \times 2.162$ MHz, and $P = -2\pi \times 4.945$ MHz^{S24}. The flip-flop between electron and nuclear spins are suppressed by the large energy mismatch. We have

$$H_{\text{NV}} \approx DS_z^2 - \gamma_e B_z S_z + P I_z^2 - \gamma_N B_z I_z + A^\parallel S_z I_z + \sum_{m_s=0, \pm 1} |m_s\rangle \langle m_s| h_{m_s}, \quad (\text{S19})$$

where the nitrogen operators

$$h_{+1} = \frac{(A^\perp)^2}{D - \gamma_e B_z} (|0_N\rangle \langle 0_N| + |-1_N\rangle \langle -1_N|), \quad (\text{S20})$$

$$h_0 = \frac{(A^\perp)^2}{-D + \gamma_e B_z} |+1_N\rangle \langle +1_N| + \left[\frac{(A^\perp)^2}{-D + \gamma_e B_z} - \frac{(A^\perp)^2}{D + \gamma_e B_z} \right] |0_N\rangle \langle 0_N| - \frac{(A^\perp)^2}{D + \gamma_e B_z} |-1_N\rangle \langle -1_N|, \quad (\text{S21})$$

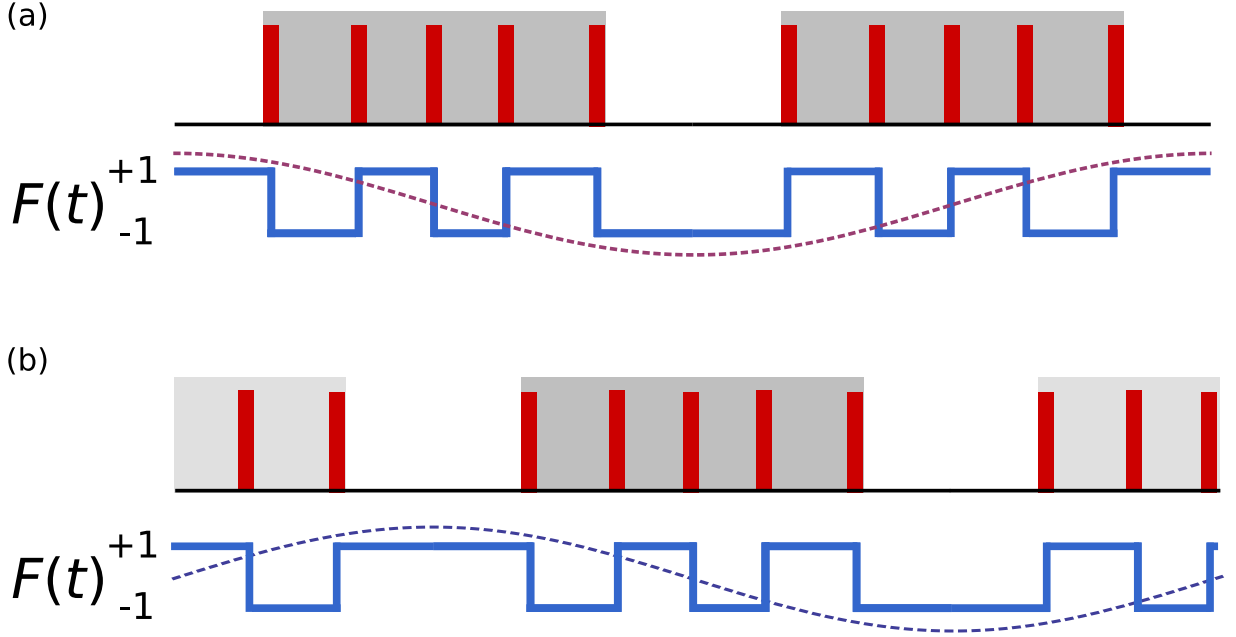


Figure S3: **Illustration of AXY pulse sequences in one period.** (a) Symmetric version and its corresponding modulation function shown below. (b) The anti-symmetric counterpart. Each of the shaded areas with a heavier colour highlights a composite π pulse in the AXY sequences. The dashed lines indicate the sinusoidal signals on-resonant to the modulation function $F(t)$.

$$h_{-1} = \frac{(A^\perp)^2}{D + \gamma_e B_z} (|0_N\rangle\langle 0_N| + |+1_N\rangle\langle +1_N|), \quad (\text{S22})$$

describe the energy shifts caused by virtual spin flip-flop processes.

We use the electron-nitrogen coupling to implement the entangled gate $u_{zz} = \exp(i\frac{\pi}{4}\sigma_z\sigma_{N,z})$ in a short duration of $0.23 \mu\text{s}$, where $\sigma_{N,z}$ is the Pauli operator of the nitrogen qubit. The iSWAP gate $\text{iSWAP} = u_{yy}u_{xx}$, where $u_{xx} = P_y u_{zz} P_y^\dagger$ and $u_{yy} = P_x u_{zz} P_x^\dagger$. Here P_α denotes decoherence-protected single-qubit $\pi/2$ gates^{S23} on both nuclear and electron spins at the α direction. The SWAP gate can be realized by $\text{SWAP} = e^{-i\pi/4} u_{zz} \text{iSWAP}$.

We simulate the SWAP gate using the protocol and achieve a gate fidelity of $F = 0.987$ (defined by $F = |\text{Tr}(GU_g)|/|\text{Tr}(GG^\dagger)|$ with G the evolution of ideal SWAP gate and U_g the actual implementation) by taking into account the energy shifts on the electron and nitrogen qubits. The microwave π pulses for the SWAP gate have pulse duration of 12.5 ns, and the field strength for rf $\pi/2$ pulses is 15.53 G. The magnetic field $B_z = 0.467$ T and the LG decoupling are the same as those used in Fig. 3b in the main text. In the simulation, we adopt the Hamiltonian Eq. (S18) and the electron and nuclear spins feel all the control fields irrespective to their frequencies. Because of the high gate fidelity, we use the nitrogen spin levels $m_N = 0, +1_N$ to store the NV electron qubit by ideal swap gates in producing the figures in the main text that use the nitrogen spin as quantum memory.

After the swap operation, the NV electron spin is polarized to the state $|+1\rangle$ for the delay window. During this storage, we take into account the energy shifts on the nitrogen memory. The energy shifts can also be removed by applying DD (e.g., a Hahn echo) on the nitrogen spin.

B. Storage to carbon-13 memory qubits

We can use AXY sequences^{S2} to implement $u_{\alpha\alpha}$ gates and swap the NV electron states to a ^{13}C memory. Compared to traditional sequences, AXY exhibits especially good spin addressability, strong robustness against detuning and amplitude errors, and the ability to continuously tune the effective interactions between NV electron and nuclear spins^{S2}. Using a symmetric version of AXY sequence (see Fig. S3 (a)), we have the interaction Hamiltonian $H_{\text{int}}^x \approx \frac{1}{4} f_{k_{\text{DD}}}^s A_j^\perp \sigma_z I_j^x$ ^{S2}. Similarly, for anti-symmetric sequences (see Fig. S3 (b)), we have $H_{\text{int}}^y \approx \frac{1}{4} f_{k_{\text{DD}}}^a A_j^\perp \sigma_z I_j^y$. We tune $f_{k_{\text{DD}}}^s = f_{k_{\text{DD}}}^a = f_{k_{\text{DD}}}$ and use a time $t_g = 2\pi/(f_{k_{\text{DD}}} A_j^\perp)$ to implement the operation

$$\text{iSWAP} = X_{\pi/2} \exp(-iH_{\text{int}}^y t_g) X_{\pi/2}^\dagger Y_{\pi/2}^\dagger \exp(-iH_{\text{int}}^x t_g) Y_{\pi/2}, \quad (\text{S23})$$

where $X_{\pi/2}$ and $Y_{\pi/2}$ are NV electron $\pi/2$ gates around the directions x and y , respectively. The inverse gate iSWAP † can be implemented by the interchanges $X_{\pi/2} \leftrightarrow X_{\pi/2}^\dagger$ and $Y_{\pi/2} \leftrightarrow Y_{\pi/2}^\dagger$.

Another way to implement the swap gate is by using continuous DD (i.e., using spin-locking field). For the addressed nuclear spin with a distinct precession frequency, we have the effective interaction Hamiltonian $H_{\text{int}} \approx \frac{1}{2}\eta A_j^\perp (\sigma_z I_j^x + \sigma_y I_j^y)$ under continuous Rabi driving (see Sec. II A). An iSWAP gate corresponds to the sequence $\exp(-i\frac{\pi}{4}\sigma_y) \exp(-iH_{\text{int}}t_g) \exp(i\frac{\pi}{4}\sigma_y)$.

In producing the figures in the main text with a ^{13}C memory, we explicitly implement the swap gate operations by ideal microwave control.

IV. SIGNALS OF DELAYED ENTANGLEMENT ECHO

A. Single spins

The evolution for a target nuclear spin is $U = e^{-i\eta A_j^\parallel \tau \sigma_z I_j^z}$ (without considering other spins) after an interaction window with time τ . Then we apply a rotation (say, along the x direction) with an angle θ_{rf} on the target nuclear spin at the delay window. Following by another interaction window with time τ between two π pulses on the electron spin (the last π pulse is optional, but we keep it for simplicity), we have a total evolution $U = e^{i\eta A_j^\parallel \tau \sigma_z I_j^z} e^{-iI_j^x \theta_{\text{rf}}} e^{-i\eta A_j^\parallel \tau \sigma_z I_j^z}$ for interaction between the NV electron spin and a target nuclear spins. Because $k_B/\hbar \approx (2\pi) \times 21$ GHz/K, the thermal energies are much larger than the nuclear spin Zeeman energies at relevant temperatures, and we approximate the thermal state of nuclear spins by the identity operator up to a normalization factor. Given the initial electron spin state $|\psi_e\rangle = (|\uparrow_e\rangle + |\downarrow_e\rangle)/\sqrt{2}$, the population left in the original equal superposition state is

$$P_{\text{NV}} = \frac{1}{2} + \frac{1}{4\mathcal{N}} \text{Tr}(U_+ U_-^\dagger + U_- U_+^\dagger), \quad (\text{S24})$$

with $U_\pm = e^{\pm i\eta A_j^\parallel \tau I_j^z} e^{-i\theta_{\text{rf}} I_j^x} e^{\mp i\eta A_j^\parallel \tau I_j^z}$ and $\mathcal{N} = 2I + 1$ the dimension of nuclear spin ($I = 1/2$ for ^{13}C). For spin- $\frac{1}{2}$, we obtain $P_{\text{NV}} = (1 + L)/2$ and the coherence $L = L(A_j^\parallel, \theta_{\text{rf}})$, where the single spin contribution

$$L(A_j^\parallel, \theta_{\text{rf}}) = \frac{1}{2} [(1 - \cos \theta_{\text{rf}}) \cos(2\eta A_j^\parallel \tau) + 1 + \cos \theta_{\text{rf}}]. \quad (\text{S25})$$

The range of single spin contribution $\cos \theta_{\text{rf}} \leq L(A_j^\parallel, \theta_{\text{rf}}) \leq 1$. When there are a number p of nuclear spins at indistinguishable Larmor frequencies, the coherence $L = L^p(A_j^\parallel, \theta_{\text{rf}})$. For the case of a $\theta_{\text{rf}} = \pi$ rotation, $L(A_j^\parallel, \theta_{\text{rf}}) = \cos(2\eta A_j^\parallel \tau)$.

B. Coupled spin pairs

Under strong magnetic field, there are three types of spin pairs^{S25}, according to their relative amplitudes between the dipolar coupling strength

$$d_{j,k} = \frac{\mu_0}{4\pi} \frac{\gamma_j \gamma_k}{|\mathbf{r}_{j,k}|^3} [1 - 3(\hat{z} \cdot \mathbf{r}_{j,k}/|\mathbf{r}_{j,k}|)^2], \quad (\text{S26})$$

and the difference of the hyperfine components $\delta_{j,k} = A_j^\parallel - A_k^\parallel$. Spin pairs with $\delta_{j,k}$ and $d_{j,k}$ the same order of strengths, which we call type-s, can be detected by DD because it modulates the electron spin coherence^{S25,S26}. This type of spin pairs can be detected by our method without application of rf driving at the delay window (i.e., $\theta_{\text{rf}} = 0$). Other types of spin pairs, type-h ($|\delta_{j,k}| \gg |d_{j,k}|$) and type-d ($|d_{j,k}| \gg |\delta_{j,k}|$), were regarded as unobservable, because their modulation on electron coherence is negligible^{S25}. Applying rf control at the delay window, we can directly detect, identify, and control type-h and -d pairs.

1. type-h pair ($|\delta_{j,k}| \gg |d_{j,k}|$)

For type-h pairs, homonuclear spin-flip processes are suppressed and therefore the precession frequency of each nuclear spin is split by d_{jk} by the internuclear interaction $H_{\text{dip}} = d_{jk} I_j^z I_k^z$. The nuclear spin flip by the rf pulse at the delay window is conditional to the state of the other spin in the nuclear spin pairs. Similar to the calculation of

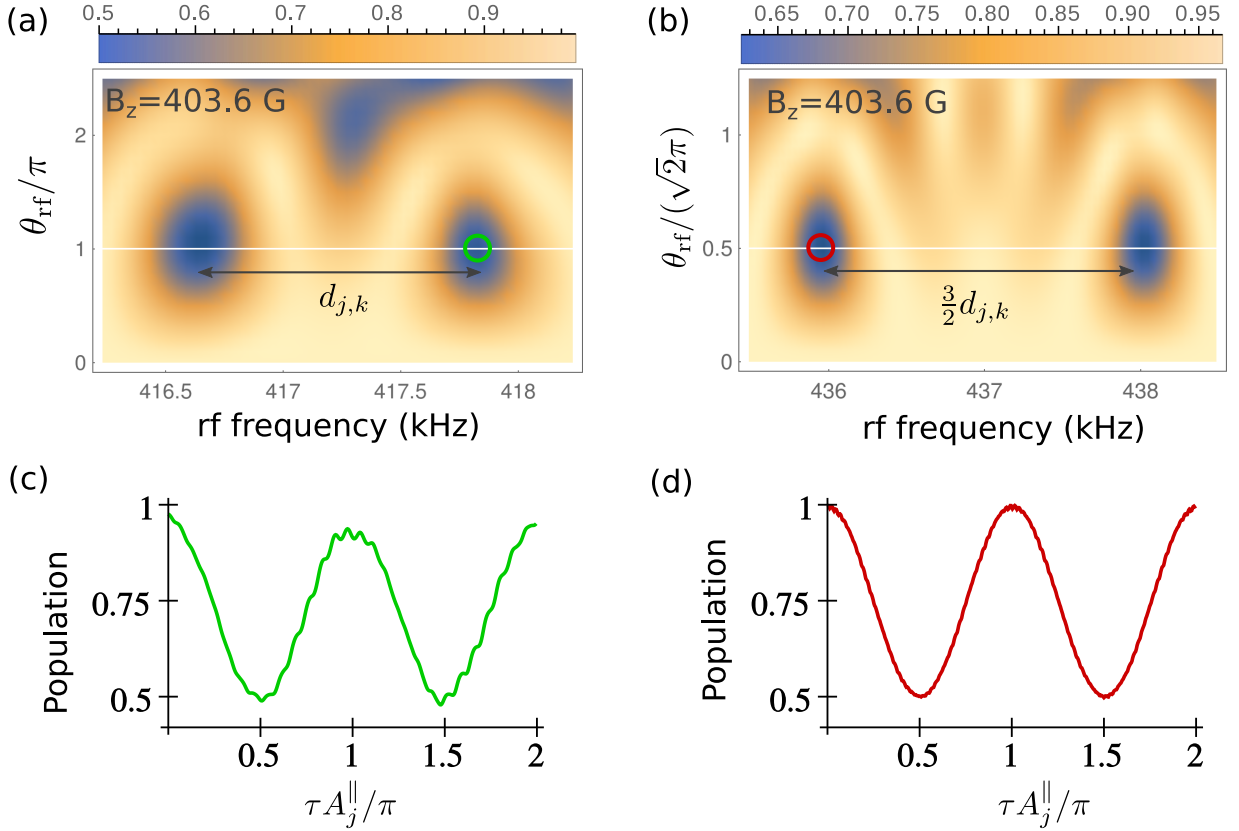


Figure S4: **Population signal of coupled spin pairs.** (a) Signal patterns of two coupled ^{13}C spins in a C-C bond ≈ 1.0 nm away from the NV centre, using the interaction time $\tau = 10 \mu\text{s}$ and rf pulse length $t_{\text{rf}} \approx 2$ ms. The dipolar coupling strength $d_{j,k} \approx 2\pi \times 1.37$ kHz. The hyperfine components of the two spins $A_j^{\parallel} \approx 2\pi \times 15.6$ kHz and $A_k^{\parallel} \approx 2\pi \times 22.5$ kHz. (b) Same as (a) but for a spin pair located ≈ 1.55 nm away from the NV centre and $\tau = 50 \mu\text{s}$, and the hyperfine components of the two spins $A_j^{\parallel} \approx -2\pi \times 5.00$ kHz and $A_k^{\parallel} \approx -2\pi \times 4.96$ kHz have similar strengths. The parameters used in (c) and (d) are indicated by the circles in (a) and (b), respectively.

single spin, when we apply a rf pulse to rotate the spin j , the population left in the original equal superposition state is

$$P_{\text{NV}} = \frac{1}{2} + \frac{1}{4\mathcal{N}} \text{Tr}(U_+ U_-^\dagger + U_- U_+^\dagger), \quad (\text{S27})$$

with $\mathcal{N} = 4$ for the dimension of the spin pair. Here $U_{\pm} = e^{-i\theta I_j^x \otimes |\uparrow\rangle\langle\uparrow|} e^{\mp i2\eta A_j^{\parallel} \tau I_j^z \otimes |\uparrow\rangle\langle\uparrow|}$ for applying a $\theta_{\text{rf}} = \pi$ spin flip on nuclear spin j conditioned on the state $|\uparrow\rangle$ of spin k . The corresponding population signal $P_{\text{NV}} = 1/2 + [1 + \cos(2\eta A_j^{\parallel} \tau)]/4 \geq 1/2$ for applying $\theta_{\text{rf}} = \pi$ on resonant to the spin j . Note that the signal is different from the case of single spin, as shown in Figs. S4 (a) and (c).

2. type-d pair ($|\delta_{j,k}| \ll |d_{j,k}|$)

For type-d pair of homonuclear spins, the interaction takes the form $H_{\text{dip}} = d_{jk}(3I_j^z I_k^z - \mathbf{I}_j \cdot \mathbf{I}_k)/2$ under a strong magnetic field^{S27}. For the nuclear spins of $I = 1/2$, the composited spin cluster has a singlet state with a composited spin $J = 0$, $|s_n\rangle = (|\uparrow\downarrow\rangle - |\downarrow\uparrow\rangle)/\sqrt{2}$. The triplet states with $J = 1$ are $|1_n\rangle = |\uparrow\uparrow\rangle$, $|0_n\rangle = (|\uparrow\downarrow\rangle + |\downarrow\uparrow\rangle)/\sqrt{2}$, and $| -1_n\rangle = |\downarrow\downarrow\rangle$. A radio frequency control $H_{\text{rf}} = \gamma_n B_x \cos(\omega_{\text{rf}} t)(I_j^x + I_k^x)$ can be written as

$$H_{\text{rf}} = \sqrt{2}\gamma_n B_x \cos(\omega_{\text{rf}} t)(|1_n\rangle + | -1_n\rangle)\langle 0_n| + \text{h.c.} \quad (\text{S28})$$

Tuning the rf frequency ω_{rf} around the splitting between $|0_n\rangle$ and $|\pm 1_n\rangle$, the nuclear spins are rotated. The nuclear state $|0_n\rangle$ has an energy of $-d_{jk}/2$, while the energies for $|\pm 1_n\rangle$ are $\pm\omega_n + d_{jk}/4$, where ω_n is the nuclear precession frequency shifted by the hyperfine field. Therefore, the transition frequencies between $|0_n\rangle$ and $|\pm 1_n\rangle$ are $\omega_n \pm 3d_{jk}/4$, shifted by the dipolar coupling. Different from the case of single spins that a spin flip requires a

rf driving time $2\pi/(\gamma_n B_x)$, here the effective rf control field is increased and transitions between $|0_n\rangle$ and $|\pm 1_n\rangle$ can be finished in a time of $\sqrt{2}\pi/(\gamma_n B_x)$. This time difference is a signature to distinguish the signals from that of single spins. Before a spin flip of the nuclear spin pair, the interaction Hamiltonian with the NV electronic spin reads $H = \eta\sigma_z(A_j^{\parallel}I_j^z + A_k^{\parallel}I_k^z)$, i.e., $H = \eta\sigma_z A^{\parallel}(|+1_n\rangle\langle+1_n| - |-1_n\rangle\langle-1_n|)$. After a time τ , we flip the electron spin and the nuclear triplet state, e.g., with a transition $|0_n\rangle \leftrightarrow |-1_n\rangle$ in a delay window. We can achieve an effective interaction $H = \eta\sigma_z A^{\parallel}(-|0_n\rangle\langle 0_n| + |-1\rangle\langle-1|)$ after the delay window. After another delay time τ , the joint evolution up to single qubit operations reads $U = \exp[-i\eta\sigma_z A_z \tau(|+1_n\rangle\langle+1_n| - |0_n\rangle\langle 0_n|)]$. The electron spin population modulated by the spin pair signal is

$$P_{\text{NV}} = \frac{1}{2} + \frac{1}{4}[\cos(2\eta A_z \tau_z) + 1]. \quad (\text{S29})$$

by using $P_{\text{NV}} = 1/2 + \text{Tr}(U_+ U_-^\dagger + U_- U_+^\dagger)/(4\mathcal{N})$ with $\mathcal{N} = 4$.

In summary for type-d pairs, the rf pulse drive the transitions between $|0_n\rangle$ and $|\pm 1_n\rangle$ of the nuclear spin triplet, with a frequency difference of $3d_{jk}/2$ and the Rabi frequency $\sqrt{2}$ times of the one for single spins, as shown in Figs. S4 (b) and (d).

Therefore the delayed entanglement echo enables the detection, identification, and control of different types of spin pairs, and it is a useful tool to extract information of more complicated spin clusters.

V. COMBINING THE INTERACTION WINDOWS WITH DYNAMICAL DECOUPLING

We can further protect the NV centre during the interaction windows with DD. Application of a DD pulse sequence (with the sequence duration τ) in an interaction window, gives the interaction of the form $H_{\text{int}} \approx (\eta/2)f_{k_{\text{DD}}}^s \sum_j' A_j^\perp \sigma_z I_j^x$ for symmetric sequences (see Sec. II A). Here the summation \sum_j' is over the spins that are not resolved by the DD sequence (with a frequency uncertainty of $\sim 1/\tau$). The interaction Hamiltonian takes the same form as the effective Hamiltonian under a strong magnetic field, but with the spin operators I_j^x instead of I_j^z (as well as the coupling constants).

In this manner, the effective interaction H_{int} during the interaction windows does not commute with the spin precession during the delay window. After the evolution during the delay window driven by $\omega_j I_j^z$, the nuclear spins could have suffered different evolutions on I_j^x because of possible differences of $\sim 1/\tau$ in their precession frequencies. This static inhomogeneous of spin precession can be removed by DD on those nuclear spins. A rf π pulse on the nuclear spins effectively reverses the evolution driven by the precession Hamiltonian $\omega_j I_j^z$. Therefore, the interaction Hamiltonians in the two interaction windows before and after the delay window are the same, when we apply a two-pulse CP sequence during the delay window. With a microwave π pulse applied on the NV electron spin before the second interaction window, the coherence of NV electron spin is preserved by the delayed entanglement echo at the end of the second interaction window.

To address desired nuclear spins, in the delay window we apply rf driving with the frequencies on the target spins to rotate the target nuclear spins. The azimuthal direction ϕ_{rf} of rf driving field is controlled by the rf phase and we choose ϕ_{rf} the same as the pulse direction of the CP sequence in the rotating frame of nuclear spin precession. When the rf driven rotation does not commute with the interaction Hamiltonian, it breaks the erasing process of delayed entanglement echo on the target spins, and thereby, we address the nuclear spins in a highly selective way. On the other hand, when the rf direction is parallel to the azimuthal angle of a target nuclear spin, the rf driving commutes with the interaction window and the electron-nuclear entanglement is removed after the echo. By measuring the rf phases ϕ_{rf} which cause vanishing signal dips, we obtain the relative directions of nuclear spins.

VI. SIMULATION DETAILS

The ^{13}C spins of the diamond samples are randomly distributed around the NV centre. In simulations for NV dynamics, we randomly distribute ^{13}C spins around the NV centre and select samples that do not contain ^{13}C nuclei within a distance of 0.714 nm from the NV centre (corresponding to 274 atomic sites), so that the hyperfine interactions between the ^{13}C nuclei and NV electron spin are simply described by the dipolar coupling Eq. (S3). The probability of getting this kind of samples is $\sim 5\%$ for natural abundance of 1.1% and is higher for lower abundances. Because of low spin concentration, simulations are accurate enough by grouping nuclear spins into interacting clusters and neglecting the intercluster interactions^{S28}. Because of the application of control fields [magnetic fields of the form $B_c \cos(\omega_c t + \phi_c)$], the total Hamiltonians for the simulations become time-dependent. To simulate the control fields, we sample the control fields in a time step of the minimum values of $0.01 \times 2\pi/\omega_c$.

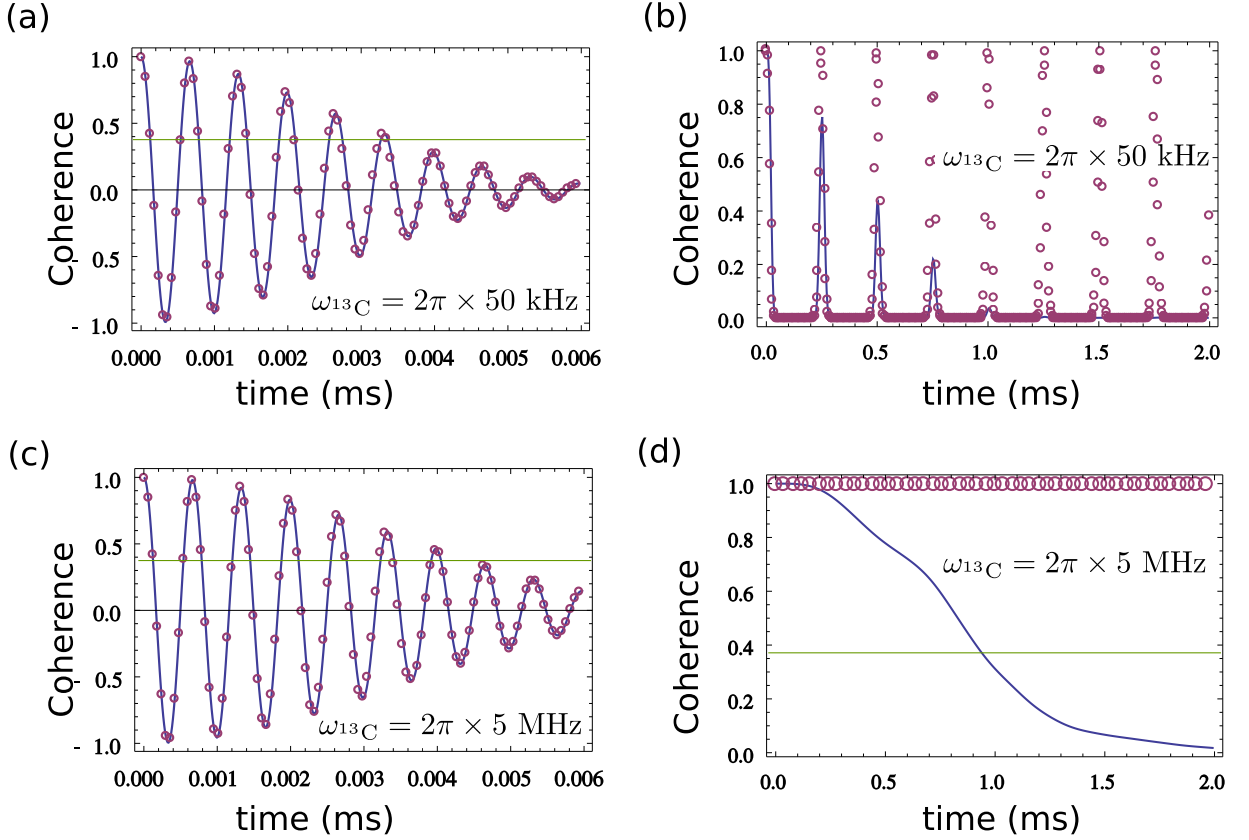


Figure S5: **Coherence of NV electron spin in interacting and non-interacting spin baths.** (a) Free evolution of the coherence (blue solid line) of NV electron spin in a spin bath used in Fig. 2 of the main text. (b) Coherence of NV electron spin with the application of a spin echo pulse at the middle of the evolution time (blue solid line). (c) As in (a), but with a much stronger magnetic field. (d) As in (b), but with a magnetic field as in (c). In (a)-(d), the circles corresponds to the case without nuclear-nuclear interactions. Under strong magnetic fields and without nuclear-nuclear interactions, the NV electron spin can have a much longer coherence time.

We adopt the coordinate system $\hat{z} = [111]/\sqrt{3}$ along the symmetry axis of NV centre and the orthogonal unit vectors $\hat{x} = [1\bar{1}0]/\sqrt{2}$ and $\hat{y} = [11\bar{2}]/\sqrt{6}$ to record the positions of ^{13}C spins $\mathbf{r}_j = [\mathbf{r}_j \cdot \hat{x}, \mathbf{r}_j \cdot \hat{y}, \mathbf{r}_j \cdot \hat{z}]$, which are measured relative to the location of the NV electron spin at the origin $[0, 0, 0]$.

The sample used for Fig. 2 of the main text contains the host nitrogen and 736 ^{13}C spins. The simulations are converged for clusters with up to 7 spins and intercluster interactions $\lesssim 2\pi \times 70$ Hz. For this sample, a spin echo π pulse extends the electron coherence times from $T_2^* \approx 4 \mu\text{s}$ to ~ 1 ms under magnetic fields much larger than the hyperfine fields at the nuclear spins (see Fig. S5), consistent with experiments^{S29} and theories^{S22}. Fig. S5 (d) also shows that the NV coherence time can be much longer if the nuclear-nuclear interactions are suppressed.

In simulations for the results of Fig. 3a of the main text, the electron spin relaxation is solved by Lindblad master equations. The signals comes from the addressing to an isolated nuclear spin located at $\mathbf{r}_j = [0.0, -1.9635, -0.8925]$ nm with the hyperfine field components $A_j^{\parallel} = 2\pi \times 1.49$ kHz and $A_j^{\perp} = 2\pi \times 2.93$ kHz. The ^{13}C memory qubit located at $[-0.714, 0.0, 0.357]$ nm has $A_m^{\parallel} = -2\pi \times 31.26$ kHz and $A_m^{\perp} = 2\pi \times 29.24$ kHz. We use AXY sequences to realize the iSWAP gate (see Sec. IIIB) on the ^{13}C qubit with a gate time $2t_g \approx 318 \mu\text{s}$, using a total number of ~ 152 composite π pulses (explicitly, 760 elementary π pulses since one composite pulse in AXY sequences has 5 elementary π pulses).

In Fig. 3b of the main text, the two spins in a C-C bond are located at $\mathbf{r}_j = [-1.2495, 0.714, -0.1785]$ nm and $\mathbf{r}_k = [-1.33875, 0.80325, -0.26775]$ nm, which imply a dipolar coupling of $d_{j,k} = 2\pi \times 1.37$ kHz. The hyperfine components $A_j^{\parallel} = -2\pi \times 4.94$ kHz and $A_j^{\perp} = 2\pi \times 5.33$ kHz for spin j , while $A_k^{\parallel} = -2\pi \times 3.72$ kHz and $A_k^{\perp} = 2\pi \times 4.2$ kHz for spin k .

In Fig. 3c of the main text, the two separated spins located at $\mathbf{r}_j = [0.0, -1.9635, -0.8925]$ nm (i.e., the target spin in Fig. 3a) and $\mathbf{r}_k = [0.0, 1.2495, 1.9635]$ nm have similar hyperfine components. The values for the second spin $A_k^{\parallel} = 2\pi \times 1.43$ kHz and $A_k^{\perp} = 2\pi \times 2.28$ kHz. We protect the interaction window with $\tau = 0.5$ ms, by using CP

sequences with 1000 microwave π pulses (corresponding to 200 composite π pulses if we use AXY sequences). The two π pulses on the ^{13}C spins are implemented by rf fields with a Rabi frequency of $2\pi \times 20$ kHz.

In the simulation with optical illumination used in Fig. 3d of the main text, we adopt the Lindblad model and parameters of the experimental paper^{S30}. The memory ^{13}C spin is similar to the one used in ref. S1, with the location $\mathbf{r}_m = [-0.108, -0.295, -1.74]$ nm and hyperfine components $A_m^{\parallel} = -2\pi \times 1.69$ kHz and $A_m^{\perp} = 2\pi \times 5.4$ kHz. We use spin lock technique on the NV electron qubit with the spin lock frequency on resonant to the precession frequency of the ^{13}C memory to perform a iSWAP gate (see Sec. III B). To implement a complete SWAP gate, we use delayed entanglement echo on the ^{13}C memory after the iSWAP operation. The delay window for the ^{13}C memory uses a 20-pulse CP sequence with duration ≈ 100 μs for a protected rf π gate. The total SWAP gate time for the simulation is ≈ 584 μs , which can be reduced by a factor of two if we use the electron levels $m_s = \pm 1$. The gate can be further protected by storing the electron state to the nitrogen spin when applying the delay window for the ^{13}C memory. Using a ^{13}C memory more strongly coupled to the NV electron can also significantly reduce the required SWAP gate times. The proton spin for detection is located 4 nm away from the NV centre, with $\mathbf{r}_j = [2.31, 2.31, 2.31]$ nm (hence $A_j^{\perp} = 0$ and the spin is hard to detect by traditional DD).

The procedure to detect the chemical shifts of proton spins with optical illumination is the following. We first pump the NV electron spin by optical field to initialize the NV electron spin to the state $|0\rangle$ with a fidelity 82% (the fidelity is obtained for the parameters in ref. S30 and it is higher for better samples), which is followed by using a swap operation to polarize the ^{13}C memory spin. Then we use optical pumping again and a microwave pulse to initialize the NV electron to a superposition state $(|0\rangle + |1\rangle)/\sqrt{2}$. After the initialization of NV electron spin and memory qubit, we let the whole system freely evolve for a time of τ to generate electron-nuclear entanglement (which can be protected by DD as shown in the main text). Then we store the NV electron spin to the memory spin by a swap gate. Subsequently we use optical illumination to decouple electron-nuclear coupling for applying a rf pulse with the length $t_{\text{rf}} \approx 80$ ms. The carry frequency of rf driving is set to the target proton spins. After optical illumination, we wait for 2 μs to relax the NV electron spin back to $|0\rangle$ state. Subsequently, we use a swap gate to retrieve the quantum state of NV electron spin and to re-popularize the ancillary ^{13}C spin. Finally, we apply a microwave π pulse on the electron spin and wait for another interaction window of time τ before readout of the electron spin state. We can increase the interaction to target spins by using the NV levels $m_s = \pm 1$, as described in the main text.

-
- [S1] Doherty, M. W. *et al.* The nitrogen-vacancy colour centre in diamond. *Phys. Rep.* **528**, 1-45 (2013).
- [S2] Casanova, J., Wang, Z.-Y., Haase, J. F. & Plenio, M. B. Robust dynamical decoupling sequences for individual-nuclear-spin addressing. *Phys. Rev. A* **92**, 042304 (2015).
- [S3] Lee, M. & Goldburg, W. I. Nuclear-magnetic-resonance line narrowing by a rotating rf field. *Phys. Rev.* **140**, A1261 (1965).
- [S4] Wang, Z.-Y., Haase, J. F., Casanova, J. & Plenio, M. B. Positioning nuclear spins in interacting clusters for quantum technologies and bio-imaging. Preprint at <http://arxiv.org/abs/1510.02811> (2015).
- [S5] Cai, J., Retzker, A., Jelezko, F. & Plenio, M. B. A large-scale quantum simulator on a diamond surface at room temperature. *Nature Phys.* **9**, 168-173 (2013).
- [S6] Kolkowitz, S., Unterreithmeier, Q. P., Bennett, S. D. & Lukin, M. D. Sensing distant nuclear spins with a single electron spin. *Phys. Rev. Lett.* **109**, 137601 (2012).
- [S7] Taminiau, T. H. *et al.* Detection and control of individual nuclear spins using a weakly coupled electron spin. *Phys. Rev. Lett.* **109**, 137602 (2012).
- [S8] Zhao, N. *et al.* Sensing single remote nuclear spins. *Nature Nanotech.* **7**, 657-662 (2012).
- [S9] London, P. *et al.* Detecting and polarizing nuclear spins with double resonance on a single electron spin. *Phys. Rev. Lett.* **111**, 067601 (2013).
- [S10] Mkhitarian, V. V., Jelezko, F. & Dobrovitski, V. V. Highly selective detection of individual nuclear spins with rotary echo on an electron spin probe. *Sci. Rep.* **5**, 15402 (2015).
- [S11] Taminiau, T. H., Cramer, J., van der Sar, T., Dobrovitski, V. V. & Hanson, R. Universal control and error correction in multi-qubit spin registers in diamond. *Nature Nanotech.* **9**, 171-176 (2014).
- [S12] Liu, G.-Q., Po, H. C., Du, J., Liu, R.-B. & Pan, X.-Y. Noise-resilient quantum evolution steered by dynamical decoupling. *Nature Commun.* **4**, 2254 (2013).
- [S13] Carr, H. Y. & Purcell, E. M. Effects of diffusion on free precession in nuclear magnetic resonance experiments. *Phys. Rev.* **94**, 630 (1954).
- [S14] Meiboom, S. & Gill, D. Modified spin-echo method for measuring nuclear relaxation times. *Rev. Sci. Instrum.* **29**, 688-691 (1958).
- [S15] Maudsley, A. A. Modified Carr-Purcell-Meiboom-Gill sequence for NMR Fourier imaging applications. *J. Magn. Reson.* **69**, 488 (1986).
- [S16] Gullion, T., Baker, D. B. & Conradi, M. S. New, compensated Carr-Purcell sequences. *J. Magn. Reson.* **89**, 479-484 (1990).

- [S17] Casanova, J., Wang, Z.-Y. & Plenio, M. B. Noise-resilient quantum computing with a nitrogen-vacancy center and nuclear spins. Preprint at <http://arxiv.org/abs/1602.06862> (2016).
- [S18] Zhao, N., Wrachtrup, J., & Liu, R.-B. Dynamical decoupling design for identifying weakly coupled nuclear spins in a bath. **90**, 032319 (2014).
- [S19] Ma, W. *et al.* Resolving remote nuclear spins in a noisy bath by dynamical decoupling design. *Phys. Rev. A* **92**, 033418 (2015).
- [S20] Loretz, M. *et al.* Spurious harmonic response of multipulse quantum sensing sequences. *Phys. Rev. X* **5**, 021009 (2015).
- [S21] Mehring, M. *Principle of High Resolution NMR in Solids* (Springer, New York, 1983).
- [S22] Zhao, N., Ho, S.-W. & Liu, R.-B. Decoherence and dynamical decoupling control of nitrogen vacancy center electron spins in nuclear spin baths. *Phys. Rev. B* **85**, 115303 (2012).
- [S23] van der Sar, T. *et al.* Decoherence-protected quantum gates for a hybrid solid-state spin register. *Nature* **484**, 82-86 (2012).
- [S24] Chen, M., Hirose, M. & Cappellaro, P. Measurement of transverse hyperfine interaction by forbidden transitions. *Phys. Rev. B* **92**, 020101(R) (2015).
- [S25] Zhao, N., Hu, J.-L., Ho, S.-W., Wan, J. T. K. & Liu, R.-B. Atomic-scale magnetometry of distant nuclear spin clusters via nitrogen-vacancy spin in diamond. *Nature Nanotech.* **6**, 242-246 (2011).
- [S26] Shi, F. Z. *et al.* Sensing and atomic-scale structure analysis of single nuclear-spin clusters in diamond. *Nature Phys.* **10**, 21-25 (2014).
- [S27] Vandersypen, L. M. K. & Chuang, I. L. NMR techniques for quantum control and computation. *Rev. Mod. Phys.* **76**, 1037 (2005).
- [S28] Maze, J. R., Taylor, J. M. & Lukin, M. D. Electron spin decoherence of single nitrogen-vacancy defects in diamond. *Phys. Rev. B* **78**, 094303 (2008)
- [S29] Cramer, J. *et al.* Repeated quantum error correction on a continuously encoded qubit by real-time feedback. Preprint at <http://arxiv.org/abs/1508.01388> (2015).
- [S30] Maurer, P. C. *et al.* Room-temperature quantum bit memory exceeding one second. *Science* **336**, 1283-1286 (2012).